Research Journal of Applied Sciences, Engineering and Technology 7(23): 4931-4939, 2014
DOI:10.19026/rjaset.7.885
ISSN: 2040-7459; e-ISSN: 2040-7467

Submitted: December 26, 2013 Accepted: January 04, 2014 Published: June 20, 2014

Research Article

Elastic Plastic Stress Distributions in Weld-bonded Lap Joint under Axial Loading

[1]Essam A. Al-Bahkali, [1, 2]Mahir H. Es-Saheb and [1]Jonny Herwan
[1]Department of Mechanical Engineering,
[2]CEREM Center of Excellence for Research in Engineering Materials, College of Engineering,
King Saud University, Riyadh 11421, P.O. Box 800, Kingdom of Saudi Arabia

Abstract: Weld-bonding process is increasingly used in many industries such like automobile and aerospace. It offers significant improvements of sheet metal joints in static, dynamic, corrosion, noise resistance, stiffness and impact toughness properties. A full understanding of this process, including the elastic-plastic stress distribution in the joint, is a must for joints design and automation of manufacturing. Also, the modelling and analysis of this process, though it is complex, proves to be of prime importance. Thus, in this study a systematic experimental and theoretical study employing Finite Element Analysis (FEA) is conducted on the weld-bonded joint, fabricated from Austenitic Stainless steel (AISI 304) sheets of 1.00 mm thickness and Epoxy adhesive Araldite 2011, subjected to axial loading. Complete 3-D finite element models are developed to evaluate the normal, shear and triaxial Von Mises stresses distributions across the entire joint, in both the elastic and plastic regions. The, needed quantities and properties, for the FE modelling and analysis, of the base metals and the adhesive, such like the elastic-plastic properties, modulus of elasticity, fracture limit, the nugget and Heat Affected Zones (HAZ) properties, etc., are obtained from the experiments. The stress distribution curves obtained are found to be consistent with those obtained from the FE models and in excellent agreement with the experimental and theoretical published data, particularly in the elastic region. Furthermore, the stress distribution curves obtained for the weld-bonded joint display the best uniform smooth distribution curves compared to those obtained for the spot and bonded joint cases. The stress concentration peaks at the edges of the weld-bonded region, are almost eliminated resulting in achieving the strongest joint.

Keywords: Adhesives, bonding, FE modelling, Heat Affected Zones (HAZ), joining, spot welding, stress distribution, weld-bonding

INTRODUCTION

Welding is a well-known fabrication process and established manufacturing technique in industry. However, weld-bonding process, which is a combination of the conventional resistance spot welding and adhesive-bonding, is increasingly used in many industries such as automobile, aerospace, home appliances etc. It offers significant improvements in static, dynamic and impact toughness properties of sheet metal joints. It improves the corrosion, noise resistance and stiffness of the joint, as shown by Ghosh and Vivek (2003). Also, it can be used for joining dissimilar materials, as reported by Yang *et al*. (2001) and later by Hasanbasoglu and Kacar (2007). Therefore, a full understanding of these processes is a must for the joints design and automation of manufacturing, particularly the bond welding process. Also, the modelling and analysis of these processes proves to be of prime importance, though it is complex.

In the last few decades, vast amount of experimental, theoretical and numerical research works is conducted and reported particularly for spot welded and adhesive bonded joints. Finite Element Analyses (FEA), 2-D and 3-D, have been widely used by many investigators in modelling these joining methods amongst them are: De *et al*. (2003), Cavalli *et al*. (2004), Li *et al*. (2005, 2006), Chen and Farson (2006), Nodeh *et al*. (2008), Kong *et al*. (2008) and later You *et al*. (2009) and Xia *et al*. (2009). However, one important aspect, which to date does not receive the needed due attention, is the knowledge of the stresses distributions at all levels of elastic and plastic loadings of these joints particularly the bond welded joints. These are required in order to assess the joint performance and application limits. This important issue is not systematically investigated neither reported in literature. Very few scattered works are reported in the elastic region only, for spot welded and bonded joints. Amongst these are the study of the stress distributions of spot welding conducted by Hou *et al*.

Corresponding Author: Mahir H. Es-Saheb, Department of Mechanical Engineering, King Saud University, Riyadh 11421, P.O. Box 800, Kingdom of Saudi Arabia

(2007) and earlier by Deng *et al*. (2000) who developed a 3-D FE model to study the stress distribution at various ratios of sheet metal thickness and spot weld nugget diameter. Recently, using FE method, stress distribution of weld-bonded steel has been plotted by Al-Bahkali *et al*. (2010). Unfortunately, little work is reported in the area of bond welding process. Therefore, to improve design procedures and welding codes, a more systematic investigation covering all stresses distributions, particularly for weld bonding, are essential. Also, achieving representative theoretical models for this process is very important in saving efforts, in the cumbersome experiments and analysis and has a positive impact on the manufacture and further design of joining.

In this investigation these issues and others are addressed. This is needed to improve the design procedures and welding codes and save efforts in the cumbersome experiments and analysis and improve the manufacture and the further design of joining. Thus, complete 3-D finite element modelling and analysis of spot welded, bonded and weld-bonded joints under axial loading is carried out and presented. Also, a comprehensive experimental program on weld-bonded joint fabricated from Austenitic Stainless steel (AISI 304) sheets of 1.00 mm thickness and Epoxy adhesive Araldite 2011, subjected to axial loading conditions is experimentally and theoretically investigated. The elastic-plastic stress distribution is determined as well as the properties and quantities of the base metals and the adhesive needed for FE modelling, such like the elastic-plastic properties, modulus of elasticity, fracture limit, the nugget and heat affected zones properties, etc. Then, the finite element models developed are used to evaluate the shear and triaxial Von Mises stresses distributions across the entire joint, in both the elastic and plastic regions. The stress distribution curves obtained, particularly in the elastic region, are compared with the published data. The details of the FEA and experimental procedures and techniques used are given in the next sections.

MATERIALS, EQUIPMENT AND EXPERIMENTAL TECHNIQUES

The material of the base metal used in this study, in the fabrication of the various joints, is Austenitic Stainless steel (AISI 304) sheet with 1.00 mm thickness. The mechanical properties of this material are found to be: Modulus of Elasticity 193.7 GPA; Yield Stress 277.3 MPa and; Ultimate Stress 729.2 MPa. These are the average values obtained from the standard tensile tests performed on three standard samples of this material according to ASTM standard E8-81 (ASTM, 1981).

The spot welding machine used in this study, for the preparation of spot welded specimen joints, is Meruit Resistance Spot Welding Machine (75 kVA). The welding electrodes are water-cooled conical copper alloy electrodes, with contact surface of 4.5 mm in diameter. The welding parameters used to fabricate the spot welded joints (Chen and Farson, 2006) are: Electrode Pressure 600 N; Welding Time 0.2 sec/cycle; Welding Current 6.5 kA and; Heat 90%.

Epoxy adhesive Araldite 2011 (from Hunstman Advanced Materials Co.) is used for bonding to fabricate both adhesive bonded and weld-bonded lap joint specimens. The mechanical properties of this adhesive as received, from Huntsman (2007) are: Flexural Modulus 1.904 GPa; Flexural Strength 60.4 MPa; Poisson Ratio 0.37; Density 1.05 g/cm^3 and; Lap Shear Strength 22 MPa. The adhesive, used for bonded and bond welded joint samples, is prepared by

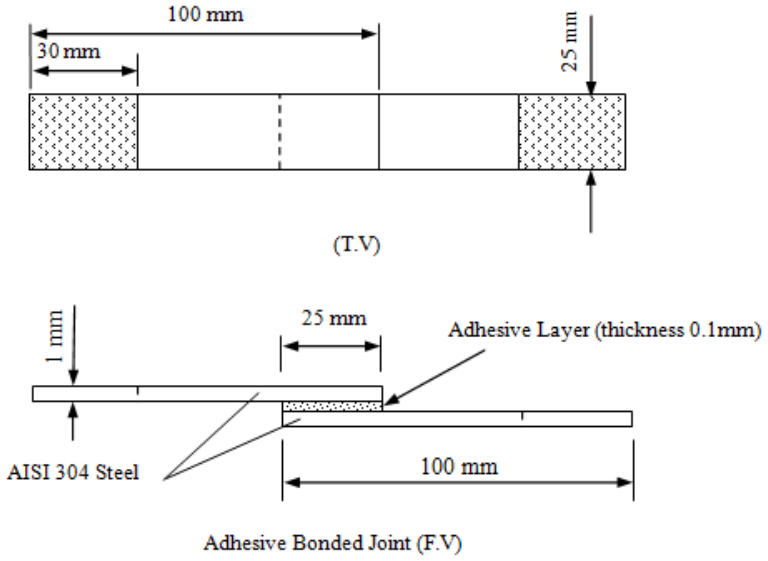

Fig. 1: Lap shear joint specimen

mechanical mixing of resin and hardener in equal amount of volume. Then, the faying surfaces were put in proper position (lap shear joint) after the application of adhesive with uniform thickness layer of 0.1 mm by manual rolling, as shown in Fig. 1. Finally the joints were cured at 120°C for 60 min to obtain coherent joints.

Again, the weld-bonded specimen joints are prepared, from the polished and cleaned stainless steel sheets, using the same techniques of the adhesive bonded joints followed immediately by resistance spot welding and subsequent curing as stated above. However, the same spot welding parameters are used, except the welding time is increased to become 0.3 sec (18 cycles) to overcome the effect of adhesive layer.

In order to obtain the needed elastic-plastic properties required by the FE modeling, micro-hardness measurements across the joint specimens are made. Vickers micro-hardness measurements of the weld nugget, heat affected zone and base metal of spot welded joints is carried out at a load of 100 g. The measurements started from the center of the nugget moving outwards step by step to the heat affected zone then the base metal, the incremental distance of 0.25 mm is used. But to obtain the plastic properties of each region, spherical indentation (using spherical indenter with 2 mm diameter) is carried out at several loads between 10 to 80 kgf. Consequently, the true stress-true strain curves for the materials in these regions are derived using Ahn-Equation, reported by Khan *et al*. (2007) and given as:

$$\sigma = \left(\frac{1}{\psi}\right) P_m = \left(\frac{1}{\psi}\right)\left(\frac{P}{\pi a_c^2}\right) \quad (1)$$

$$\varepsilon = \left(\frac{\alpha}{\sqrt{1-(a_c/R)^2}}\right)\left(\frac{a_c}{R}\right) \quad (2)$$

where,

σ = The true stress

ψ = A plastic constrain factor equal to 3.6 verified by the material tensile test

P = The load

P_m = The mean pressure

a_c = The contact radius between the indenter and the material

ε = The true strain

α = The adjustment constant taken as 0.14

R = The indenter radius

The standard shear tensile test of all lap shear joint specimens of the bonded, spot welded and weld-bonded joints is carried out on an Instron Machine (series 3385 H) at 1 mm/min crosshead speed.

Furthermore the ductile fracture limit data are needed to conduct the numerical study of fracture initiation using ABAQUS package. The data are usually expressed in terms of stress triaxialities vs. equivalent strains, as documented by many investigators such like; Mackenzie *et al*. (1977), Alves and Jones (1999), Bao (2005), Jeon *et al*. (2006) and later Sun *et al*. (2009). Therefore, to obtain these data, a series of tensile tests (five tests in total) on several notched tensile specimens and FE-Model of the tensile test of these specimens are conducted. In total, five specimens were prepared and used with notch radii varied between 2 to 5 mm. Then, the equivalent strains are determined from the tensile test data and the corresponding stress triaxialities are evaluated by the FE model.

FINITE ELEMENT MODELS AND BOUNDARY CONDITIONS

Geometry: A 3D finite element model is developed for each joint type namely: spot welded, bonded and weld-bonded as well as the base material tensile specimen. Figure 2 shows the configuration, dimensions, constraints and loading conditions for both bonded and weld-bonded models. The total length of the models used is 175 mm and each strip has a thickness of 1.0 mm.

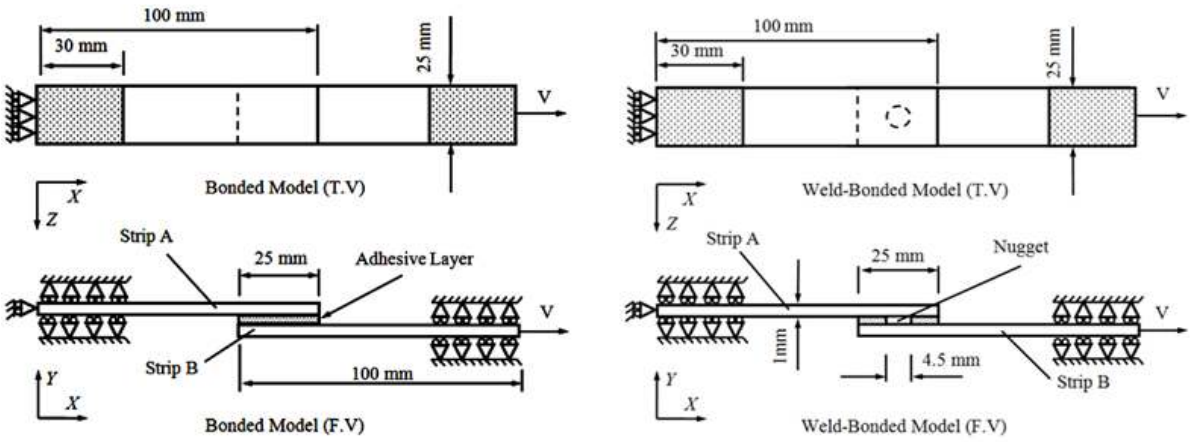

Fig. 2: Finite-element configurations for the bonded and weld-bonded joints

Analysis assumptions: Throughout the idealization process, the following assumptions were considered: The problem is modelled using three-dimensional FE analysis and due to symmetry along the center line of the joints, half of the joint is only considered to save computation time. The adhesive layer is assumed to be isotropic. The dimensions of the nugget and Heat Affected Zone (HAZ) are defined from the micro-hardness measurements. Also, the nugget size is verified from the measurements of the fractured specimen of spot welded joints. The zones are connected with each other by sharing the nodes. The elastic-plastic properties of each zone are introduced based on the material tensile test results for the base metal and the spherical indentation measurements for the nugget and heat effected zone. In order to define the fracture initiation in the FE model, the ductile fracture limit criteria is, also, introduced base on the experimental and numerical data of the notched specimen tensile test, reported by Mackenzie *et al*. (1977), Alves and Jones (1999), Bao (2005), Jeon *et al*. (2006) and later Sun *et al*. (2009) and Al-Bahkali *et al*. (2010). Finally, the adhesive layer is modeled and developed using traction separation mode, since the fracture occurred at the interface between stainless steel and the adhesive layer, (and not within the adhesive layer).

Boundary conditions: The mechanical boundary conditions associated with each finite element model developed, can be summarized as follows.

Symmetric boundary conditions are applied along the x-axis side. As a result of that, two constraints are imposed. The rotation and horizontal displacement at the line of symmetry are zero.

On the left edges at x = 0, clamped boundary conditions are imposed. Thus, the displacements become:

$$u_x|_{X=0} = u_y|_{X=0} = u_z|_{X=0} = 0 \quad (3)$$

Whereas both strips are subject to a fixed y-direction boundary condition at the first 30 mm segment of the left base metal strip A (i.e., at x = 0 to 30 mm) and at the end 30 mm segment of right base metal strip B (i.e., at x = 145 to 175 mm):

$$u_y|_{X=0-30} = u_y|_{X=145-175} = 0 \quad (4)$$

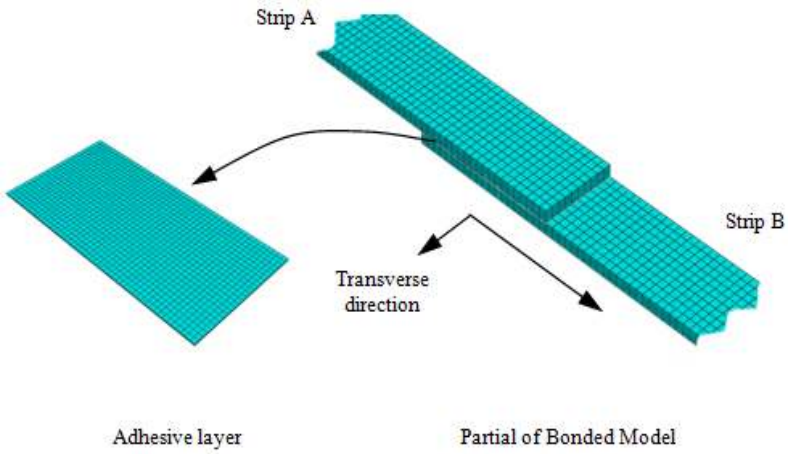

Fig. 3: Finite-element mesh for bonded joint model

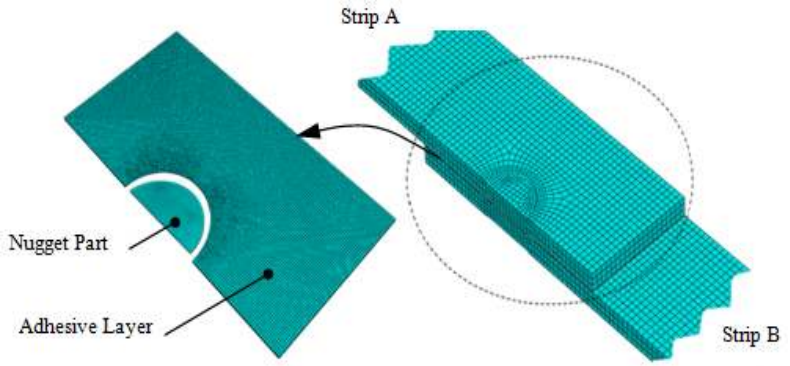

Fig. 4: Finite-element mesh for weld-bonded joint model

Table 1: Number of elements used in the different FE models

Model	Bonded	Spot	Weld-bonded
Base strips A and B	744	6972	10202
Adhesive layer	300	-	1471
Nugget	-	690	1035

The model is subjected to a constant speed of 1 mm/sec at the right edges of strip B:

$$V_x|_{X=175} = 1\text{mm/min} \quad (5)$$

Finite element mesh: The finite element computation was carried out using ABAQUS explicit (ABAQUS, 2010), (Ghosh and Vivek, 2003). The finite-element meshes of these models are generated using eight-node-linear brick reduced integration elements (C3D8R) for the stainless steel and three dimensional cohesive elements type COH3D8 for the adhesive layer. Figure 3 and 4 show the FE meshes for both bonded and weld-Bonded models respectively. The mesh of bonded model is straight forward and simpler because of the absence of spot welding and it reaches mesh independent solution with a relatively coarse mesh. However, the weld-bonded model needs additional finer mesh on the edges of spot weld and adhesive layer to avoid error analysis. The numbers of elements for the different models that used in the current study, after several refined meshes to insure the conversion of the FE results, are given in Table 1. However, for more details about the experimental and theoretical techniques and analyses used in this investigation the work by Herwan (2010) can be consulted.

RESULTS AND DISCUSSION

Load-displacement curves:

FE and experimental results of spot-welded joints: Figure 5 shows the complete load-displacement curves obtained from the FE model and the corresponding experimental results derived from the actual test carried out on the spot-welded joint. It is clear that, the FE results are in good agreement with the experimental results, though at the plastic region a maximum acceptable error of 2.6% was observed.

FE and experimental results of bonded joints: The load-displacement curves obtained from the adhesive-bonded joint shear tensile tests are shown in Fig. 6. Again, the experimental and FE results are found to be identical and show good agreement, particularly at the elastic region and fracture initiation (de-lamination) point. A maximum, acceptable error of 3.82% at the middle of the plastic region was observed, though mesh refinement was employed to eliminate or reduce its effect. But, in general the obtained experimental and FE deformation shapes after de-lamination were in good agreement.

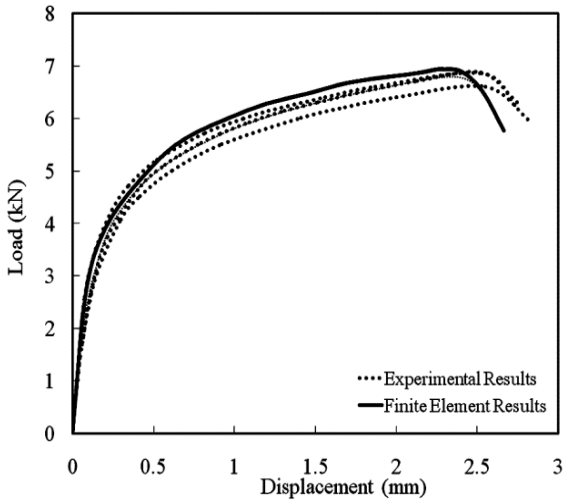

Fig. 5: The FE and experimental results of the spot-welded joint

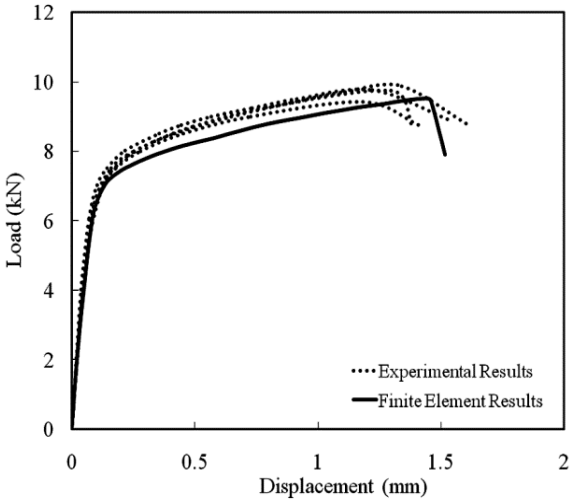

Fig. 6: The FE and experimental results of the bonded joint

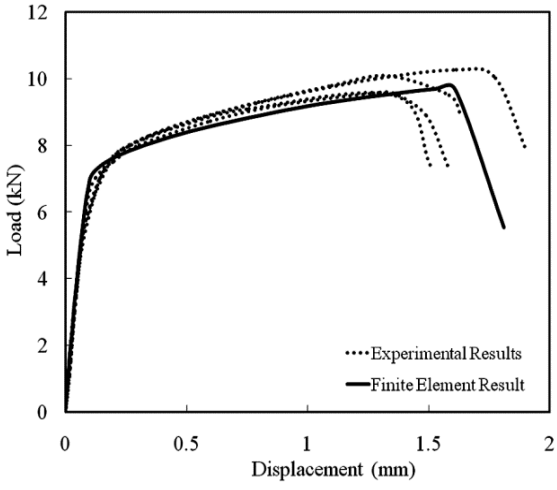

Fig. 7: The FE and experimental results of weld-bonded joint

FE and experimental results of weld-bonded joints: As stated above, the FE model of the weld-bonded joint was developed by combining the spot-welded and adhesive-bonded joint models. Figure 7 shows the obtained experimental and FE results. Again, excellent agreement between the FE results and experimental data at all regions (i.e., elastic, plastic and fracture initiation point) is observed. This is due to the comprehensive utilization of the model developed from the actual experimental joint data.

The stresses distribution for spot, bonded and weld-bonded joint: The stress distributions were recorded and calculated at several axial load levels (i.e., elastic, plastic region and fracture point), as shown in Table 2. Meanwhile, the elastic and plastic stress distribution curves for the various loading conditions and different joints are displayed in Fig. 8 to 10.

Table 2: Axial load levels at which stress distributions are recorded

Range	Spot welded	Bonded	Weld-bonded
Load within elastic	280	290	288
limit (N)	3282	3324	3257
	-	5709	5712
Load within plastic	5756	6880	6868
limit (N)	6882*	9001*	9006*

*: Fracture limit load for the model

Figure 8 shows the normal stress distributions σ_y, the shear stress distribution τ_{xy} and the Von Mises stress distributions $\sigma_{V.M}$, in a spot welded joint under axial loading at different levels of elastic loading (two levels of elastic loading) and plastic loading (one level at the ultimate loading). The abscissa is in X/L, where X presents the position of the obtained stresses from left to right of the lap joint and L is the length of lap join

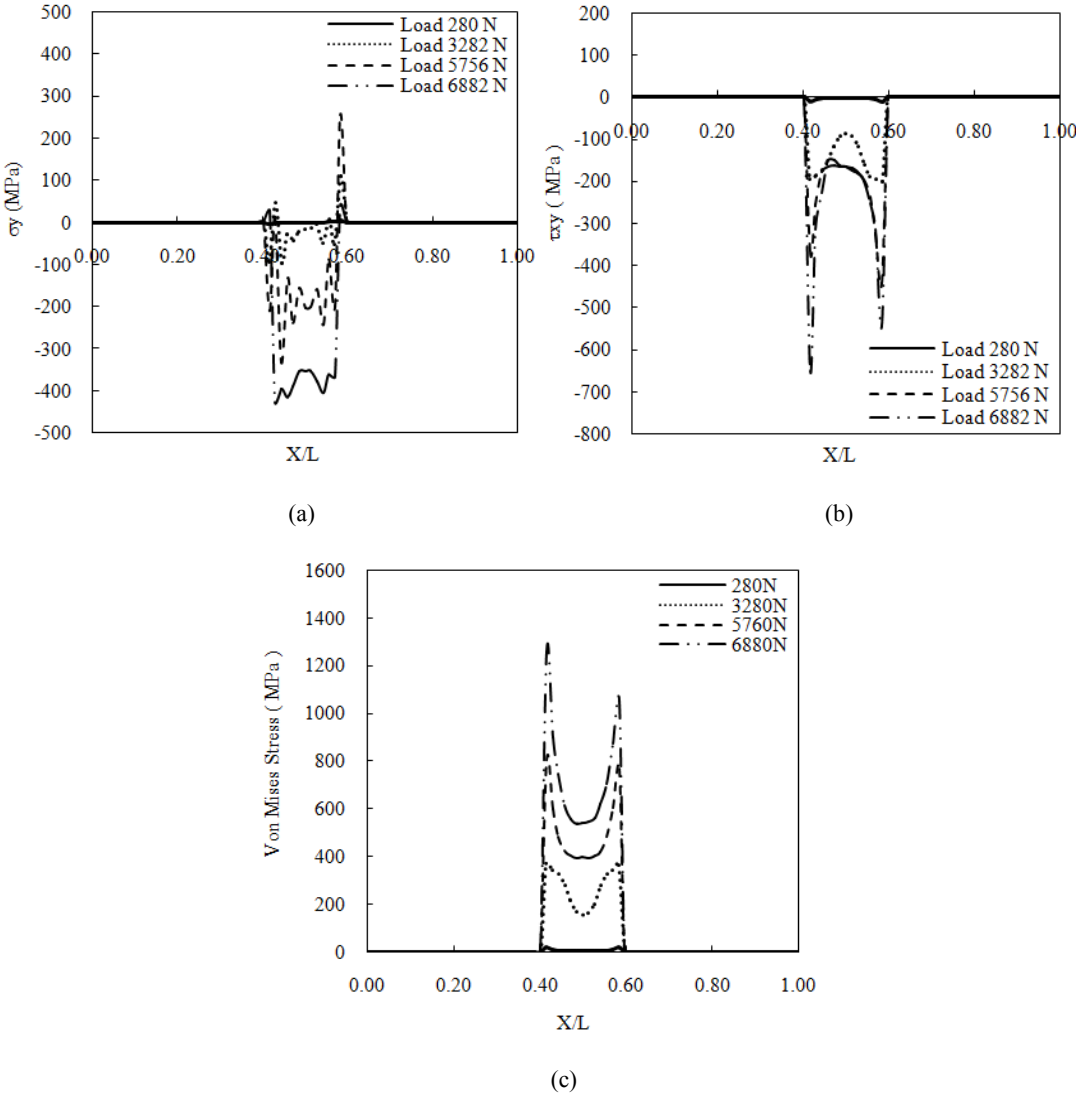

Fig. 8: Elastic-plastic stresses distribution plots for spot welded joint at the different elastic and plastic loading levels, (a) the normal stress distribution (σ_y), (b) shear stress distribution (τ_{xy}), (c) the Von Mises stress distributions ($\sigma_{V.M.}$)

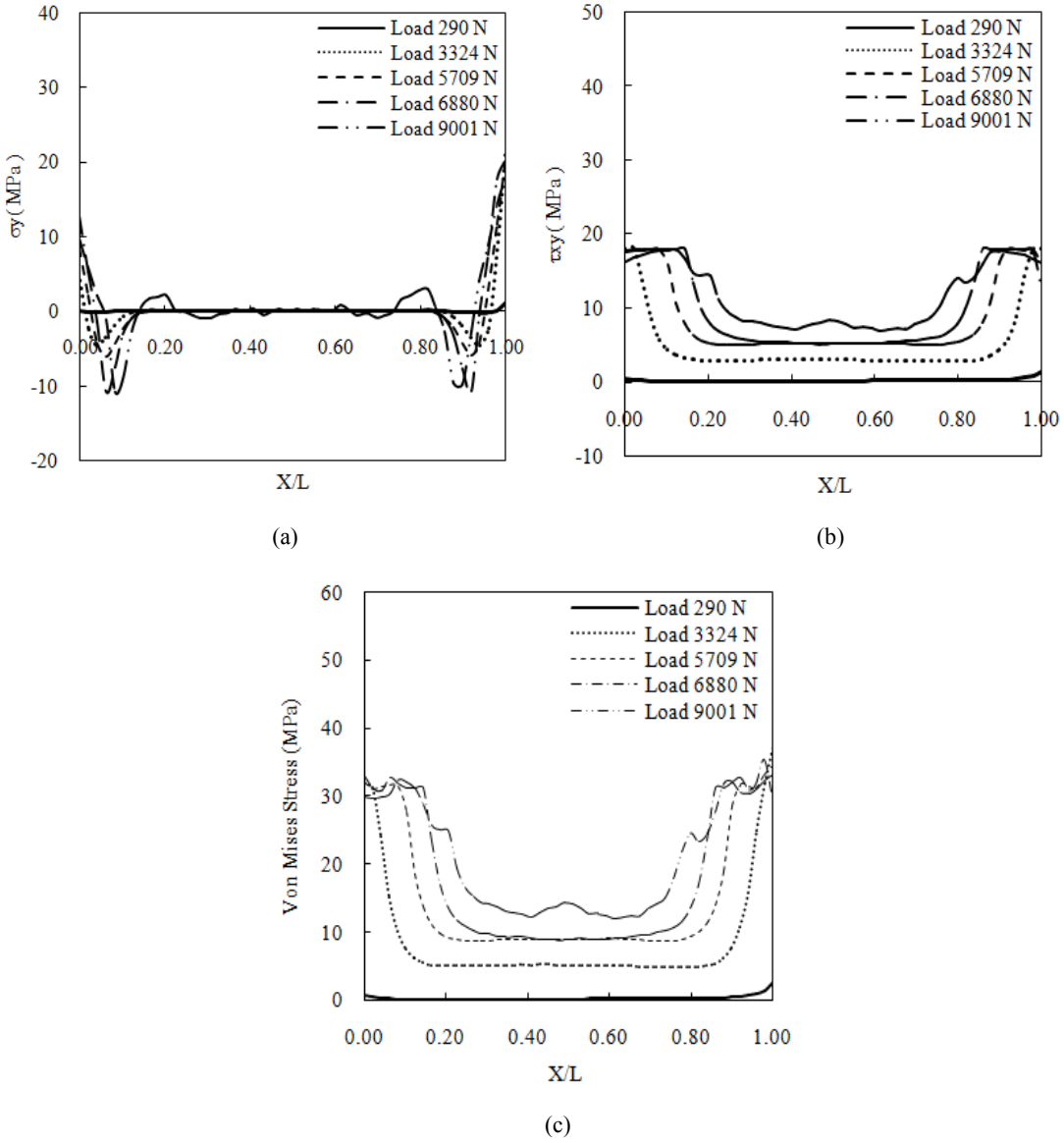

Fig. 9: Elastic-plastic stresses distribution plots for bonded joint at the different elastic and plastic loading levels, (a) the normal stress distribution (σ_y), (b) shear stress distribution (τ_{xy}), (c) the Von Mises stress distributions ($\sigma_{V.M.}$)

(25 mm). Figure 9 shows, similar elastic and plastic stress distribution curves obtained in bonded joint under axial loading at different levels of elastic loading (three loading levels below elastic limit and two loading levels above the elastic limit). Again, similar arrangements for elastic and plastic stress distributions obtained in the weld-bonded joint are displayed in Fig. 10. The curves in this case are given at different axial loading levels, (three loading levels below the elastic limit and two above it). It is clear from all these curves that the stress distributions obtained in the weld-bonded joints, shown in Fig. 10 are more uniform and the edges peaks of stresses are almost eliminated compared with those obtained in the spot welding and adhesive bonding cases shown in Fig. 8 and 9 respectively.

It is noticed that, the failure of spot welded joints is taking place at the interface between the weld-nugget and HAZ. This can be attributed to the fact that the Von Mises stress and normal stress in x-direction are very high at these positions, as shown in Fig. 8. But, in the adhesive bonded joint, the failure (i.e., load drop) tends to start whenever the shear stress at the interface between adhesive and base metal reaches the maximum value of 18 MPa, nearly at 30% of the area of the lap-joint. This is observed to happen at the axial loading of about 9 kN, as shown in Fig. 9. Thus, the adhesive joint continue to carry the load below this value, since the area under maximum shear stress still not reaching the critical 30% of the total lap joint area. Also, it is found that the effect of adhesive in the weld bonded joint is

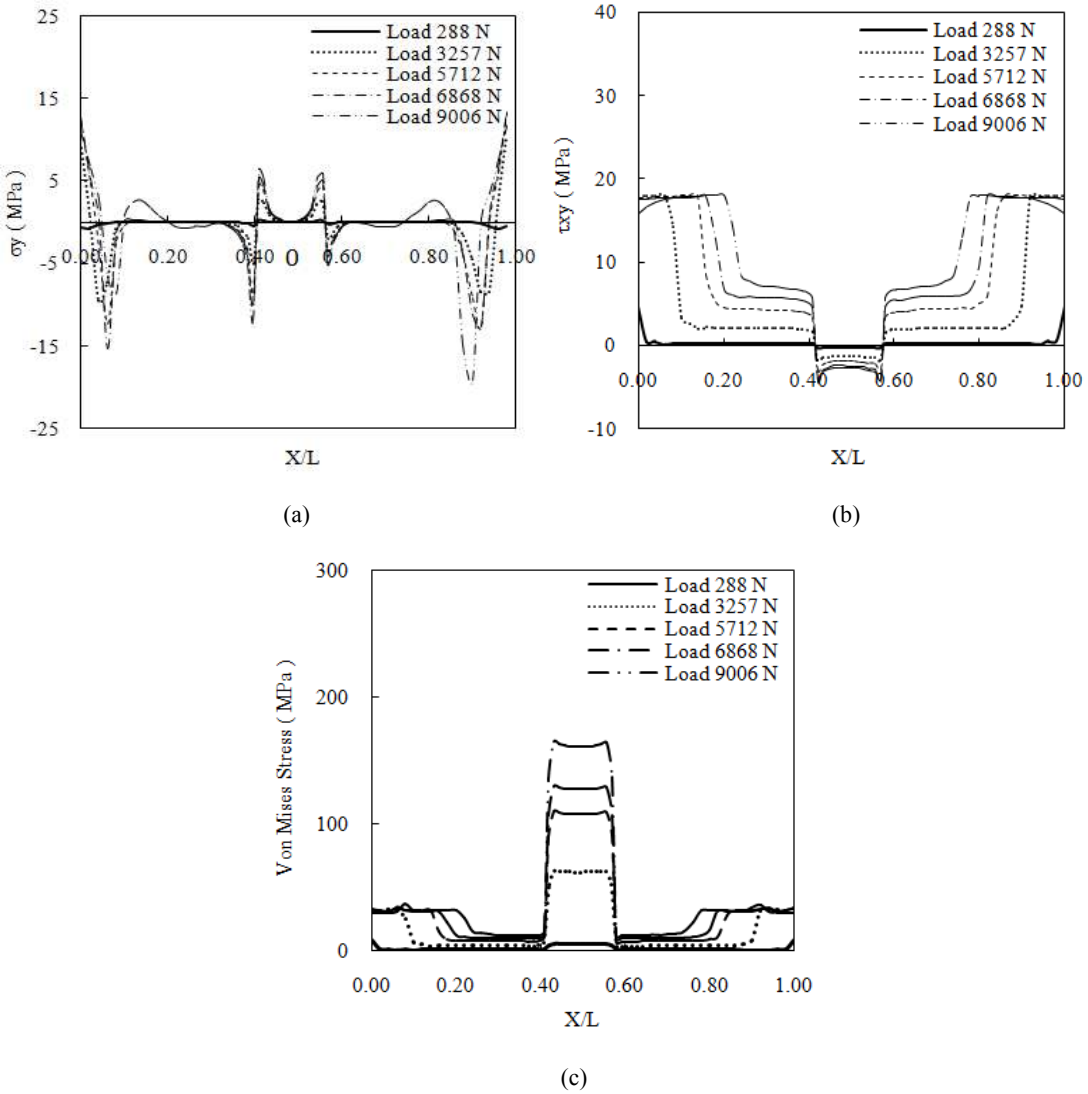

Fig. 10: Elastic-plastic stresses distribution plots for weld-bonded joint at the different elastic and plastic loading levels, (a) the normal stress distribution (σ_y), (b) shear stress distribution (τ_{xy}), (c) the Von Mises stress distributions ($\sigma_{V.M.}$)

significantly reducing the maximum stress surrounding the nugget area as show in Fig. 10. Meanwhile, the existence of the nugget strengthen the adhesive joint, as reflected in the increased area with maximum shear stress from 30% (in the adhesive joint case) to 40% in this case (i.e., weld-bonded case). This explains the reason why the weld-bonded joint possesses the highest strength amongst the three types of joints. Furthermore, it is clear from stress distribution curves that the stress distribution obtained in the case of weld bonded joints, shown in Fig. 10 is more uniform and the edges peak stresses are almost eliminated compared with those obtained in the spot welded and adhesive bonded cases (Fig. 8 and 9). Finally, the weld-bonded joint displayed the highest resistance to deformation and failure and offering the highest maximum load carrying capacity (Fig. 10).

CONCLUSION

The 3D FE modelling of the three types of spot welded, adhesive bonded and weld bonded joints are successfully achieved. The load-displacement curves of all three joining types are, also, successfully obtained. In all cases excellent agreement between the results of the FE models and the experimental results are displayed. The deformation modes, fracture initiation point and complete load-displacement curves obtained by the FE models show excellent agreement with the experimental data. Finally, using proper FE models, the elastic and plastic stress distributions were successfully simulated in term of normal stress, shear stress and Von Mises stress at several axial loading levels. All results obtained compared well with the experimental results and very strongly agree with the published data. The weld-bonded joint showed the highest carrying load

capacity with the best performance and uniform stress distributions without any stress concentration peaks. Finally, the results of this investigation are believed to have positive impact on the manufacture and the further design of joining as well as improving design procedures and welding codes and save efforts in the cumbersome experiments and analysis.

ACKNOWLEDGMENT

The authors are grateful for the Center of Excellence for Research in Engineering Materials (CEREM) at KSU, for the support of this study (Project No. 430-CEREM-08).

REFERENCES

ABAQUS, 2010. User's Manual. Version 6.9. Retrieved from: http://abaqusdoc.ucalgary.ca/v 6.9/.

Al-Bahkali, E., M. Es-Saheb and J. Herwan, 2010. Finite element modelling of weld-bonded joint. Proceeding of the 4th International Conference on Advanced Computational Engineering and Experimenting, Paris.

Alves, M. and N. Jones, 1999. Influence of hydrostatics stress on failure of axi-symmetric notched specimens. J. Mech. Phys. Solids, 47: 643-667.

ASTM, 1981. Standard Method of Tension Testing of Metallic Materials. Annual Book of ASTM Standard, ASTM-E8-81.

Bao, Y., 2005. Dependence of ductile crack formation in tensile tests on stress triaxiality stress and strain ratios. J. Eng. Fract. Mech., 72: 502-522.

Cavalli, M.N., M.D. Thouless and Q.D. Yang, 2004. Cohesive-zone modeling of the deformation and fracture of weld-bonded joints. Weld. J., 83: 133S-139S.

Chen, J.Z. and D.F. Farson, 2006. Analytical modeling of heat conduction for small scale resistance spot welding process. J. Mater. Process. Tech., 178: 251-258.

De, A., M.P. Thaddeus and L. Lorn, 2003. Numerical modeling of resistance spot welding of aluminum alloy. ISIJ Int., 43(2): 238-244.

Deng, X., W. Chen and G. Shi, 2000. Three-dimensional finite element analysis of the mechanical behavior of spot welds. Finite Elem. Anal. Des., 35: 17-39.

Ghosh, P.K. and R. Vivek, 2003. Weld-bonding of stainless steel. ISIJ Int., 43: 85-94.

Hasanbasoglu, A. and R. Kacar, 2007. Resistance spot welding of dissimilar materials (AISI 316L-DIN EN 10130-99). J. Mater. Design, 28: 1794-1800.

Herwan, J., 2010. Load-displacement curve prediction of weld-bonded stainless steel using finite element method. M.Sc. Thesis, King Saud University, KSA.

Hou, Z., I.S. Kim, Y. Wang, C. Li and C. Chen, 2007. Finite element analysis for the mechanical features of resistance spot welding process. J. Mater. Process. Tech., 185: 160-165.

Huntsman, C., 2007. Technical Data Sheet of Structural Adhesives Araldite-2011. Huntsman Advanced Materials. Retrieved from: www.intertronics. co.uk/data/ara 2011.pdf.

Jeon, E., J.Y. Kim, M.K. Baik, S.H. Kim, J.S. Park and D. Kwon, 2006. Optimum definition of true strain beneath a spherical indenter for deriving indentation flow curves. J. Mater. Sci. Eng., A419: 196-201.

Khan, I., M.L. Kuntz, Y. Zhou, K. Chan and N. Scotchmer, 2007. Monitoring the Effect of RSW Pulsing on AHSS Using FEA (SORPAS) Software. SAE Technical Paper 2007-01-1370, DOI: 10.4271/2007-01-1370.

Kong, X., Q. Yang, B. Li, G. Rothwell, R. English and H.J. Ren, 2008. Numerical study of spot-welded joints of steel. J. Mater. Design, 29: 1554-1561.

Li, S., M.D. Thouless, A.M. Waas, J.A. Schroeder and P.D. Zavattieri, 2005. Use of mode I cohesive zone models to describe the fracture of an adhesively-bonded polymer-matrix composite. J. Compos. Sci. Technol., 65: 281-293.

Li, S., M.D. Thouless, A.M. Waas, J.A. Schroeder and P.D. Zavattieri, 2006. Mixed-mode cohesive-zone models for fracture of an adhesively bonded polymer-matrix composite. J. Eng. Fract. Mech., 73: 64-78.

Mackenzie, A.C., J.W. Hancock and D.K. Brown, 1977. On the influence of state of stress on ductile failure initiation in high strength steels. J. Eng. Fract. Mech., 9: 167-188.

Nodeh, I.R., S. Serajzadeh and A.H. Kokabi, 2008. Simulation of welding residual stresses in resistance spot welding, FE Modeling and X-ray verification. J. Mater. Process. Tech., 205: 60-69.

Sun, C., M.D. Thouless, A.M. Waas, J.A. Schroeder and P.D. Zavattieri, 2009. Rate effects for mixed-mode fracture of plastically-deforming adhesively-bonded structures. Int. J. Adhes. Adhes., 29: 434-443.

Xia, Y., Q. Zhou, P.C. Wang, N.L. Johnson, X.Q. Gayden and J.D. Fickers, 2009. Development of high-efficiency modeling technique for weld-bonded steel joints in vehicle structures-part I: Static experiments and simulations. Int. J. Adhes. Adhes., 29: 414-426.

Yang, Q.D., M.D. Thouless and S.M. Ward, 2001. Elastic-plastic mode-II fracture of adhesive joints. Int. J. Solids Struct., 38: 3251-3262.

You, M., Z. Li, X. Zheng, S. Yu, G. Li and D. Sun, 2009. A numerical and experimental study of performed angle in the lap zone on adhesively bonded steel single lap joint. Int. J. Adhes. Adhes., 29: 280-285.